Modeling CO_2 flow in support of a shallow subsurface controlled leakage field test

Rodrigo S. Iglesias[1]*; Cristiane Romio[2]; Clarissa L. Melo[1]; Ana Paula S. Musse[3]; Fátima do Rosário[3]; Curtis M. Oldenburg[4]

[1]*Instituto do Petróleo e dos Recursos Naturais (IPR) – Pontifícia Universidade Católica do Rio Grande do Sul (PUCRS) – Av. Ipiranga 6681, Porto Alegre – 90619-900 – Brazil*

[2]*Department of Engineering - Biological and Chemical Engineering, Aarhus Univerisity, 8200 Aarhus, Denmark*

[3]*PETROBRAS - CENPES Centro de Pesquisas e Desenvolvimento Leopoldo Américo Miguez de Mello, 21941-915, Rio de Janeiro, RJ, Brazil*

[4]*Energy Geosciences Division – Lawrence Berkeley National Laboratory, Berkeley, CA 94720, USA.*

* corresponding author

Note: This manuscript is published and should be cited as follows:

Iglesias, R.S., Romio, C., Melo, C.L., Musse, A.P.S., do Rosário, F. and Oldenburg, C.M., 2019. Modeling CO2 flow in support of a shallow subsurface controlled leakage field test. *Greenhouse Gases: Science and Technology, 9*(5), pp.1027-1042.

Abstract

Controlled release of CO_2 into the soil and atmosphere is performed to test detection and monitoring tools, for which several field laboratories were established by a number of institutions worldwide. Numerical simulations of CO_2 behavior in the shallow subsurface region are another form of validation and verification of the leakage pathways and destinations. These studies aim to improve monitoring and verification of CO_2 in case of unexpected leakages, for public assurance. In this work we present the results of a numerical modeling study conducted to simulate the injection of CO_2 as carried out during a field test in Viamão, southern Brazil, where 20 kg/d of CO_2 were pumped for 30 days through a vertical

well 3 m below ground in a altered granitic soil. Multiphase flow simulations were performed with the TOUGH2/EOS7CA software for unsaturated porous media, using field data and injection parameters, including sensitivity tests to permeability direction, diffusivity, and boundary conditions. Results with increased horizontal permeabilities are in better agreement with the field observations. In this condition, mass balance calculations indicate approximately 90% of injected CO_2 (20 kg/day during 30 days) remains in the soil after 180 days from injection start, consistent with the measured flow through the soil-atmosphere interface.

Keywords: CCUS; CO2; Modeling; TOUGH2; EOS7CA

1. Introduction

Carbon capture, utilization and storage (CCUS) is one of the widely recognized solutions for minimizing carbon dioxide (CO_2) concentrations in the atmosphere, either by CO_2 removal or avoiding CO_2 emissions from large-scale sources. Among the possible permanent sinks for the captured CO_2, geological reservoirs are the most interesting ones, due to their worldwide availability and their immense storage capacity.[1–5] The reservoirs that are currently considered as the most viable options - deep saline formations and depleted oil&gas reservoirs – have a likely estimated capacity of over a thousand gigatonnes of CO_2, enough for storing many decades of anthropogenic emissions[2,6].

Even though geological storage is already a proven technology at the scale of a single site, new methods and tools for tracking and monitoring CO_2 during and after injection, are constantly being developed. Nevertheless, technologies are mature enough and have been proven in numerous projects at different scales, demonstrating containment and compliance to regulations. [7–10] A variety of methods have been successfully tested, and numerical simulations provided validation through history-matching monitored data with remarkable accuracy.[10–14] Monitoring and simulation tests and validations are invaluable not only for ensuring the reservoir itself is performing, but also for the natural and manmade environment that can be affected by potential leakage of CO_2 from the reservoir. This includes the shallow surface region (soil and aquifers) and atmosphere that can be reached by leakage through wells or geological faults and fractures in the overlying formations.[10,15] In order to better understand near-surface CO_2 leakage behavior and related monitoring, several field-scale CO_2 release experiments have been implemented in the near-surface environment at various sites around the world[16–22]. Among the first and most important ones is the ZERT[16], in Montana (US), where several experiments were carried out during summer periods from 2007-2014, using a shallow (ca. 3 m) horizontal well for CO_2 release. Other relevant experiments include

the Ginninderra[17] (Australia, 2010), with the longest running injection (up to 80 days); the CO2FieldLab[18] in Norway (2011), one of the deepest injection wells (20 m, at 45° inclination) and highest injection rates; the CO_2-Vadose project[19], in France, where CO_2 was injected in a limestone quarry and the PISCO2[23] in Spain, where CO_2 was injected in artificially constructed tanks filled with soil. Further details and information on these experiments, among others, can be found in comprehensive reviews published recently by Ko et al. (2016)[24] and Roberts et al (2017)[7].

Numerical modeling studies based on some of the previously mentioned experiments were performed as well. The ZERT experiment was modeled using the TOUGH2/EOS7CA software to predict the injection rate and design monitoring strategies.[25] The same code was used to simulate different injection scenarios (injection rates, soil characteristics, weather events) within the PISCO2 project[23], and also the injection of nitrogen and CO_2 in the Maguelone site in France (as part of the SIMEx project).[26] The PHREEQC code[27] was used to model changes in water composition with CO_2 injection and dissolution during the field experiment at the CO_2FieldLab site in Norway.[28] All studies report that the simulations as an effective tool for validation of monitoring methods and calibration of experimental parameters.

In Brazil, since 2011, two joint R&D projects have been developed under the full sponsorship of PETROBRAS with CO_2 controlled releases in monitored field laboratories. The first one, the Ressacada Project, finished in 2015, while the second one (CO_2MOVE Project)[29] started in the same year in the city of Viamão (Figure 1).

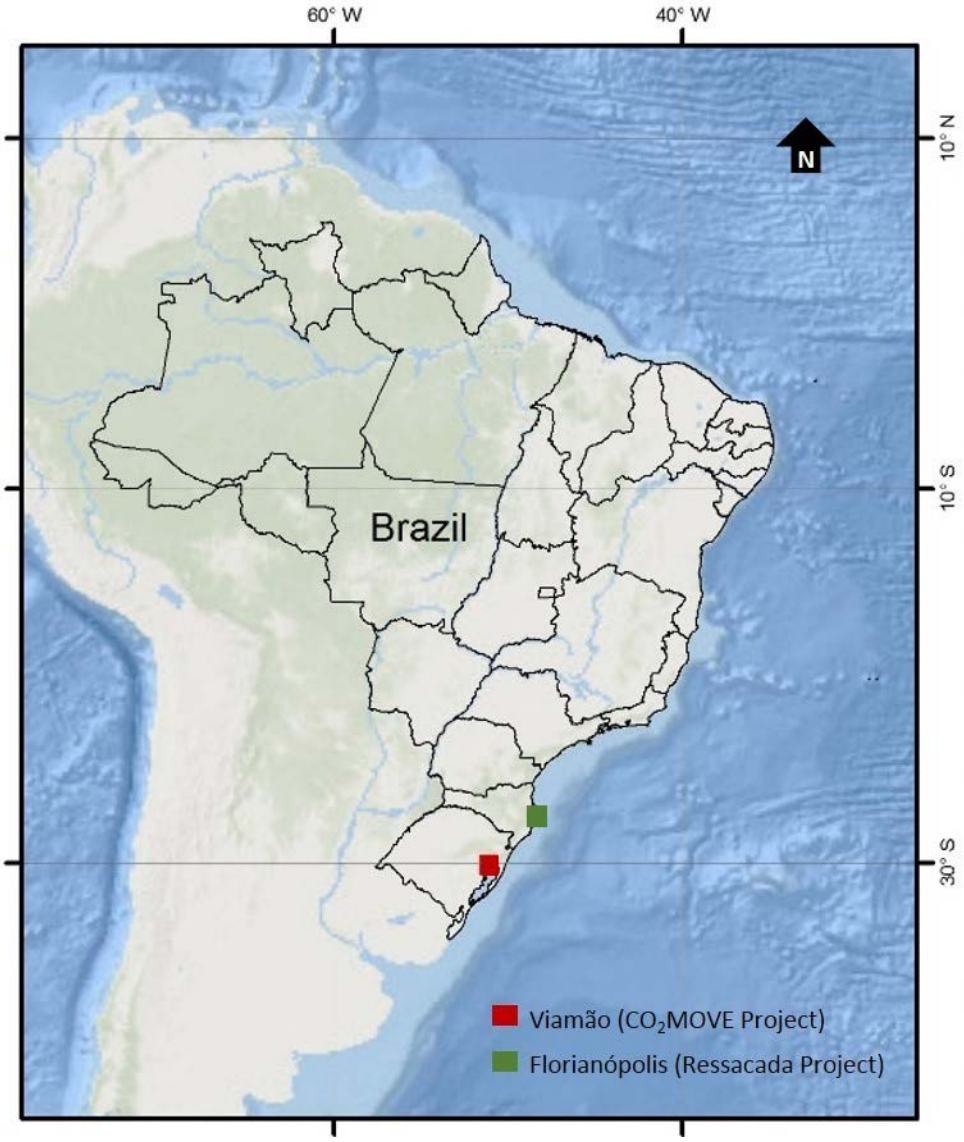

Figure 1. Location of the two Brazilian CO_2 monitoring field labs. Ressacada Farm in Florianópolis city is indicated by the green square and the CO2MOVE site in Viamão city is indicated by the red square (adapted from Melo et al.[29]).>

The first CO_2MOVE field experiment was conducted in 2016 over 60 days, of which the first 15 days were for pre-injection surveys, followed by 30 days of CO_2 injection. The last 15 days were for post-injection measurements. The gas was injected through a vertical well at 3 m depth, positioned in the lowest region of the site (NE), in a heterogeneous argillaceous soil (regolith), with rates of up to 20 kg/day. The site was extensively characterized prior to

injection, by drilling a series of wells (up to 10 m deep). Characterization included granulometric analyses of the sediments, hydraulic conductivity, and water level monitoring. Additional information and results of the site characterization and leakage experiment are described by Melo *et al*, 2017.

In order to design and interpret the field CO_2 release results, numerical models were used to simulate subsurface CO_2 flows on the site. In this paper, we present the results of these simulations, using data obtained from the characterization of the study area and operating conditions of the experiment. Fluid flows were simulated using multiphase flow and transport equations for unsaturated porous media as implemented in the TOUGH2/EOS7CA software[30,31]. Simulations were conducted including sensitivity tests for a few conditions such as permeability anisotropy, diffusivity, and boundary conditions.

2. Materials and Methods

2.1. Numerical tools

Simulations were conducted using TOUGH2,[32] developed for solving multiphase multicomponent flow and transport in porous media. The specific TOUGH2 equation of state module used in this study was EOS7CA,[30] designed for shallow unsaturated media with the components air, a non-condensable gas (CO_2 in this case), an optional tracer, and water. The model grid and input was built using the PetraSim pre-processing software for the TOUGH2 family of codes. For visualization of results, TecPlot 360 software was employed.

2.2. Model definitions and properties

The model geometry and properties were defined using data obtained from the Viamão field site.[29] The modeled area is ca. 3,500 m^2, and is shown in Figure 2 by the white outline.

Figure 2. Aerial view of the Viamão site where the CO2MOVE Project is being developed. The study area is highlighted in white (adapted from Melo et al.[29]).>

For modeling purposes, a 3D site geological model was created using RockWorks software, based on stratigraphic profiles obtained from shallow characterization holes drilled in the area along with soil analyses. In this first stage of simulations, we approximated the system as being composed of five homogeneous layers with varying thickness and inclination (SW-NE slope), and an unconfined aquifer despite the heterogeneous character of the regolith as shown in Figure 3. The properties of the soil layers as measured by standard granulometric methods[33] is presented in Table 1.

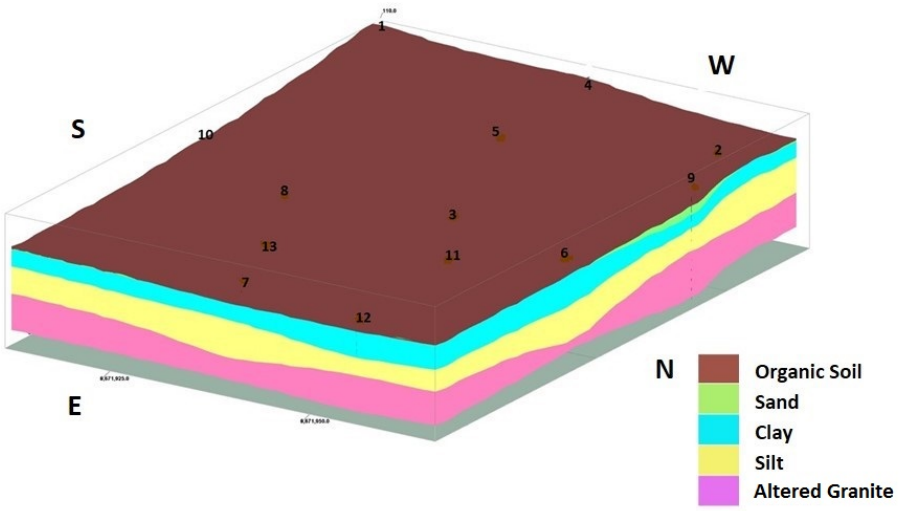

Figure 3. Geological model built for the study area. Colors represent different material layers. Numbers indicate soil sampling and/or monitoring wells (adapted from Melo et al.[29])>

Table 1: Soil physical properties summary.

Material	**Porosity[1] (%)**	**Permeability[2] (m^2)**	**Specific mass ($kg.m^{-3}$)**	**Clay content (%)**	**Sand content (%)**
ORGANIC SOIL	0.55	4.99×10^{-12}	400	28.3	52.1
SAND	0.25	1.80×10^{-11}	1400	27.6	57.7
CLAY	0.50	3.94×10^{-10}	1250	38.2	44.8
SILT	0.20	1.26×10^{-10}	1760	30.6	45.6
ALTERED GRANITE	0.11	3.79×10^{-11}	2300	25.2	45.1

[1]Estimated from granulometry using SPAW software; [2]From hydraulic conductivity

The two-phase flow properties, relative permeability and capillary pressure, are calculated using the model equations shown in Table 2. Some of the equation parameters were estimated from the clay and sand content of each layer (Table 1) using methods incorporated into the Soil-Water Characteristics tool of the SPAW Hydrology software, from the U.S. Department of Agriculture.[34]

Table 2: Multiphase flow equations and parameters determined for each layer.

Material	Relative permeability (van Genuchten-Mualem model) $k_{rl} = \begin{cases} \sqrt{S^*}\left\{1-\left(1-[S^*]^{\frac{1}{\lambda}}\right)^{\lambda}\right\}^2 & if\ S_l < S_{ls} \\ 1 & if\ S_l \geq S_{ls} \end{cases}$ $k_{rg} = \begin{cases} 1 - \mathrm{k_{rl}} & if\ S_{gr} = 0 \\ \left(1-\hat{S}\right)^2\left(1-\hat{S}^2\right) & if\ S_{gr} > 0 \end{cases}$ $S^* = (S_l - S_{lr})/(S_{ls} - S_{lr})$ and $\hat{S} = (S_l - S_{lr})/(1 - S_{lr} - S_{gr})$				Capillary pressure (van Genuchten model) $P_{cap} = -P_0\left([S^*]^{-\frac{1}{\lambda}} - 1\right)^{1-\lambda}$ $S^* = (S_l - S_{lr})/(S_{ls} - S_{lr})$				
	λ	S_{lr}	S_{ls}	S_{gr}	λ	S_{lr}	$1/P_o$	P_{max}	S_{ls}
ORGANIC SOIL	0.31	0.41	1	0.05	0.31	0.4	5.0×10^{-5}	1.499×10^{6}	1
SAND	0.2	0.36	1	0.05	0.2	0.35	3.0×10^{-4}	1.466×10^{6}	1
CLAY	0.3	0.56	1	0.05	0.3	0.55	3.5×10^{-5}	1.481×10^{6}	1
SILT	0.24	0.36	1	0.05	0.24	0.35	6.0×10^{-5}	1.467×10^{6}	1
ALTERED GRANITE	0.26	0.31	1	0.05	0.26	0.3	7.0×10^{-5}	1.488×10^{6}	1

The geological model was exported to PetraSim, resulting in a 68.5 m (*x*) × 52 m (*y*) × 12.3 m (*z*) size structure. The model grid was built by dividing the structure into 34, 27, and 23 divisions in the *x*, *y*, and *z* directions, respectively, totaling approximately 21,100 cells. Most cells consist of rectangular blocks of 2.31 m × 2.31 m × 0.52 m. The region surrounding the injection well was refined, dividing the *x* and *y* lengths by 2, resulting in 1.115 m × 1.115 m × 0.52 m cell blocks. The whole model was considered isothermal, at 20 °C. The resulting model grid is presented in Figure 4A.

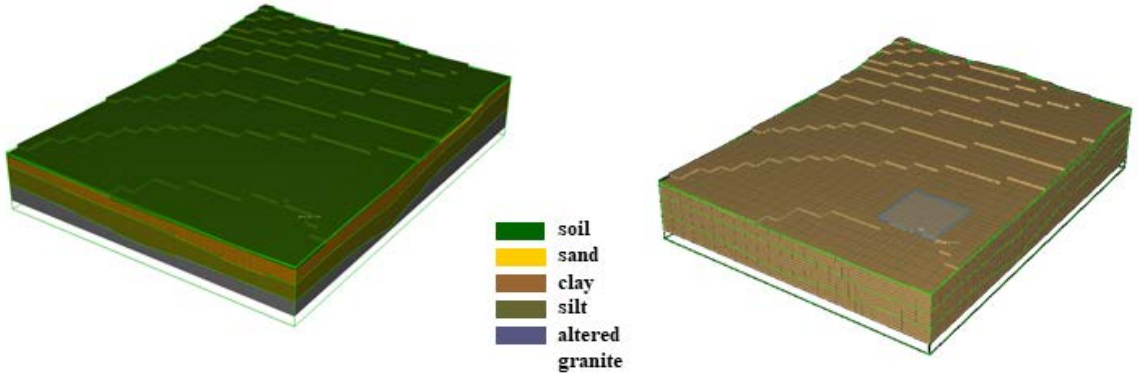

Figure 4. (A) Model grid layers of different materials; (B) grid refinement around the injection point.

2.3. Simulation procedures

Prior to injection simulations, the 3D model system was initialized by performing a gravity-capillary equilibration procedure. In short, the aqueous phase is pulled downward by gravity and upward by capillarity in an unsaturated system, and this equilibration process results in a variable distribution of aqueous phase saturation in the unsaturated zone. When doing injection simulations in such as this system, it is necessary to generate this static phase saturation distribution prior to simulating CO_2 injection. The equilibration procedure involves defining an artificial water table layer with water and air saturations fixed at 0.5, with zero capillary pressure and full mobility for all phases, ensuring the exchange of fluids with the upper part of the model. Above the water table, saturations of water and air also start at 0.5 (initial values are not relevant since the final saturation distribution will be defined by the capillary pressure model and its parameters). Below the water level, the system was fully saturated with water. Following this initial run in which a static gravity-capillary equilibrium was reached with acceptably low flow rates (e.g., flow rates in the model less than ca. 10^{-7} kg/s), the resulting saturations and pressures are defined as the input for the next step, where the special water table layer is reassigned normal soil properties and the bottom boundary is

set to hold conditions of pressure and saturation fixed at the values calculated during the gravity-capillary equilibrium run. Another static gravity-capillary equilibration is run following which the system is ready for simulating CO_2 injection.

The injection of CO_2 was carried out through a single cell representing the injection well located at x = 51.3 m, y = 39.8 m and z = 102.5 m (z coordinate relative to sea level, corresponding to a 3.1 m depth relative to the model surface). The injection cell is located in a silt layer (Figure 5B), 1.6 m below the water table (z = 104 m). Water table level was estimated after monitoring in the field, indicating an average of 1 m below surface at the injection point during dry seasons.[29] Matching the field experiment, injection of CO_2 was carried out for 30 days, with a constant rate of 20 kg/day. After completing the injection, the simulation was allowed to run for an additional 5 months (180 days of simulation in total).

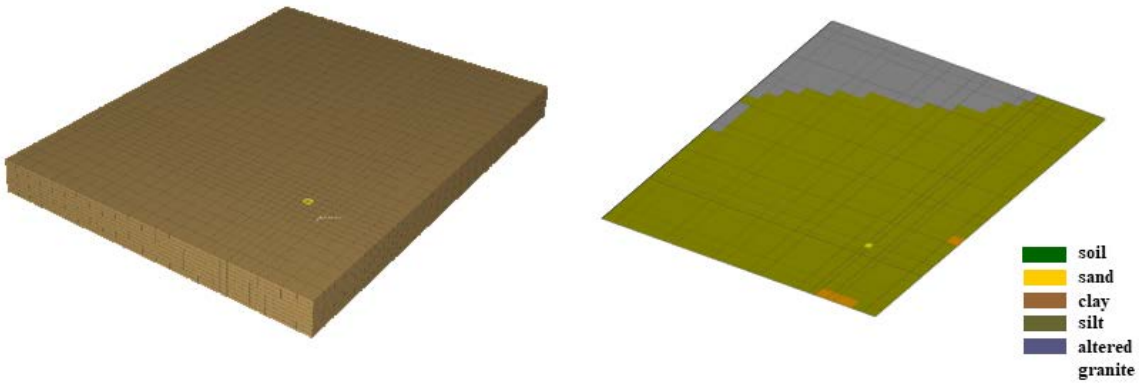

Figure 5. (A) Injection cell (yellow) – cells above injection plane are not shown; (B) model slice at injection point (yellow) showing grid block material types (z = 104 and 1.6 m below the water table).

Simulations were also carried out testing some parameter variations for studying sensitivities. The effect of diffusion was verified by running the simulations both with and without molecular diffusion. When diffusion was included, the diffusivity coefficient was defined as 10^{-5} m^2/s for gas phases and 10^{-10} m^2/s for the liquid phase. The effect of permeability anisotropy was evaluated by testing three different conditions: a) isotropic permeability (k_x = k_y = k_z); b) anisotropic permeability with 10-times increase in the x and y directions (k_x = k_y =

$10k_z$) and c) anisotropic permeability with 10-times decrease in the z-direction ($k_x = k_y = k_z/10$). These conditions were tested with the no-diffusion model. Finally, different boundary conditions were considered for the top of the model (surface-atmosphere limit). As a base case, the top boundary was considered open to flow (a more realistic scenario). This is done by adding an extra layer of grid blocks to the top representing the atmosphere, with small cell height and saturations calculated for 100% relative humidity at 20 °C (to avoid evaporation processes that would tend to dry out the system). This layer is set with Dirichlet-type boundary conditions, i.e., fixed properties (temperature, pressure, saturation) and open for fluid flow. For comparison of boundary effects and mass balances, additional simulations were carried out with a closed top boundary (no atmosphere layer). This case was modeled without diffusion and isotropic permeabilities.

3. Results and Discussion

Following the gravity-capillary equilibration procedures, the distribution of saturation used as the initial condition for CO_2 injection was obtained as shown in Figure 6.

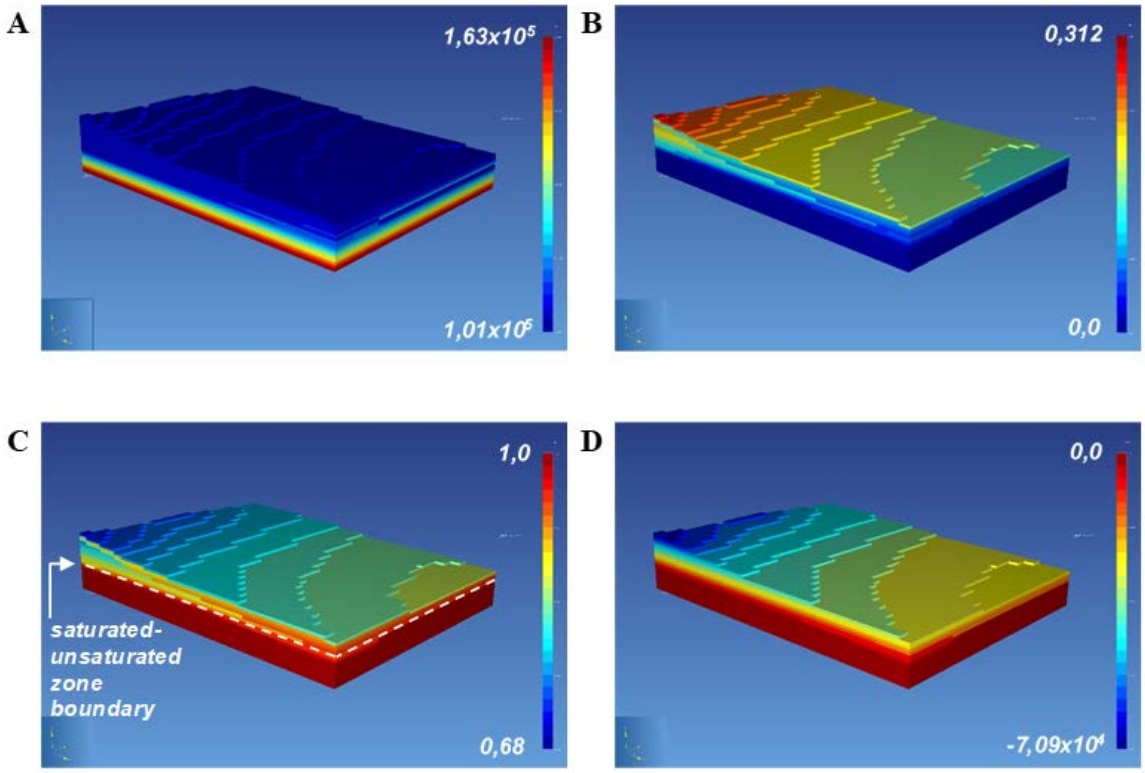

Figure 6. Distribution of pressure (A), gas saturation (B), liquid saturation (C), and capillary pressure (D) in the model after gravity-capillary equilibration steps.

The maximum residual flowrates of ca. 10^{-7} kg/s persisting from the gravity-capillary equilibration process are located well within the model interior, along the boundary between the silt and clay layers and the zone of transition between the regular and refined grid around the well. Fluids flow in a very slow steady-state circular motion within this region. These small flows arise frequently in irregular grids due to virtual hydraulic head differences between vertically and horizontally displaced grid blocks that arise from the limited finite precision of the inter-grid block distances and orientation of connection lines with respect to gravity. These slow flows do not substantively affect the injection simulation, as the injection rates are at least three orders of magnitude larger than the maximum flowrates at the quasistatic equilibrium state (20 kg/day $\approx 10^{-4}$ kg/s vs. 10^{-7} kg/s).

For the base case (open top boundary, without diffusion and isotropic permeability), the shape of the CO_2 plume at 30 days (end of injection) and at 180 days after injection begins is

presented in Figure 8, by means of three isosurfaces at 0.95, 0.5 and 0.05 CO_2 molar fraction of gas phase, and cross sections at the injection point. The CO_2 plume is irregularly shaped, as it flows through several materials with different properties, as well as through grid blocks of different sizes. At 30 days, the plume has reached well into the top of the model. From the vertical (y-z plane) cross-section, it is visible that the plume is divided in two parts. This is likely the result of horizontal spreading movement before the gas reaches the upper (clay) layer, which has higher porosity and provides a faster flow both horizontally and vertically. Comparing results at 30 and 180 days, it is clear that the CO_2 plume remains nearly stagnant after injection stops, which is expected as there are no ongoing perturbations or significant intrinsic driving forces in the model that cause advective flow, and diffusion is not included. In the aqueous phase, there is a delay as CO_2 takes more time to dissolve. In 30 days, the CO_2-rich water region is smaller than the gas plume and more concentrated around the injection point. After 180 days, CO_2 dissolves further in the liquid phase and occupies a similar region as the gas phase (Figure 8, bottom row). Despite having a much lower mass fraction of the aqueous phase (less than 0.22%), most of the CO_2 injected is rapidly solubilized in water, ending up being ca. 95% in this phase (see Figure 11B), as liquid saturations are much higher than gas phase saturations in most of the model.

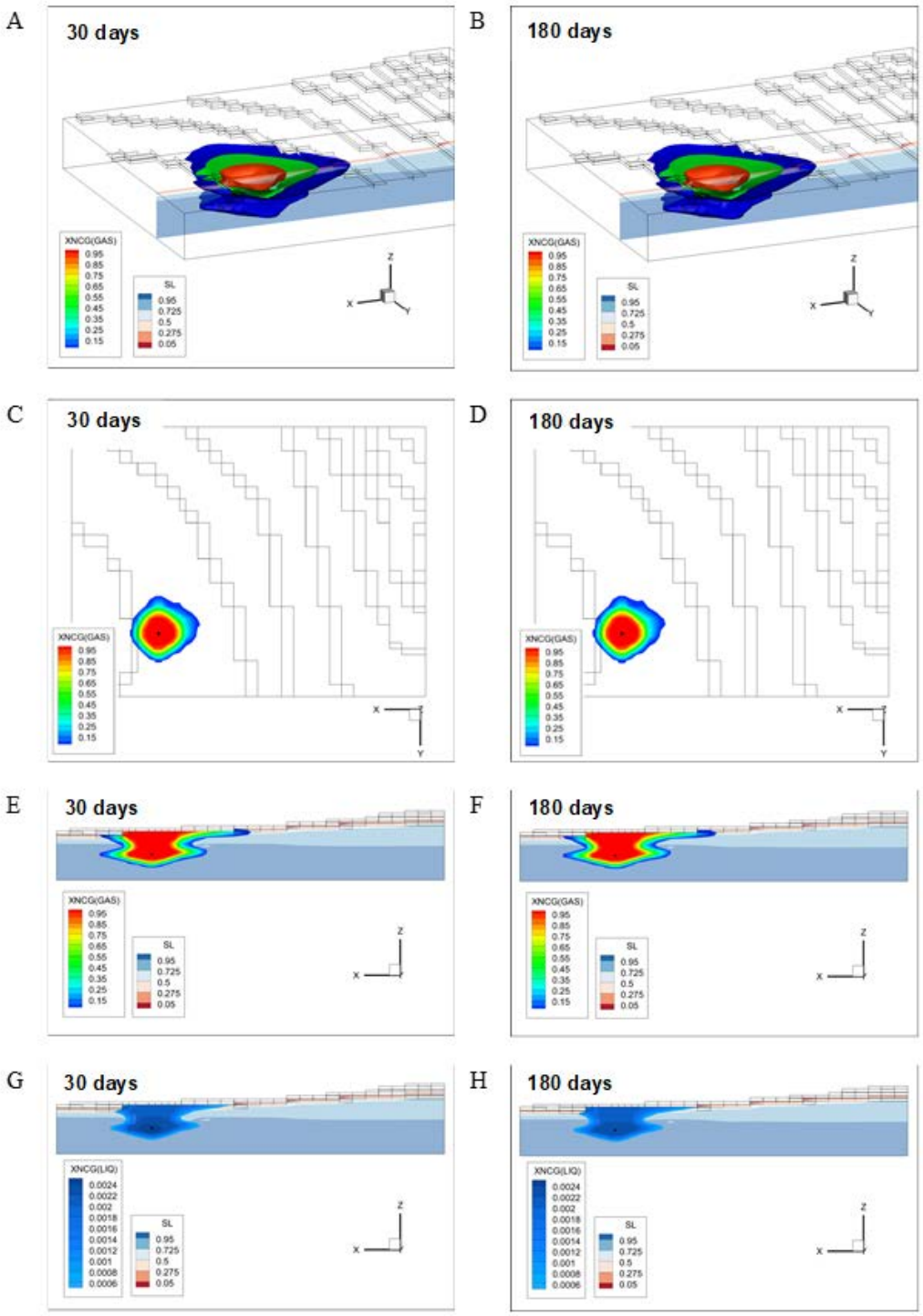

Figure 7: Figure 7. CO_2 mass fraction in the gas phase (A–F) and liquid phase (G and H) at 30 days (left column) and 180 days (right column) after injection onset. (A and B) 3D isosurfaces at 0.95 (red), 0.5 (green), and 0.05 (blue) mass fractions; (C and D) horizontal cross-section at injection point; (E and F) vertical cross-section at injection point; (G and H) CO_2 mass fraction in the liquid phase (SL, liquid phase saturation).

When diffusion is included, the plume behaves quite differently, especially after injection stops. At 30 days, there are no perceived differences when diffusion is included, as the flow

is mostly dominated by advection due to injection overpressure. At 180 days, the effect of diffusion is quite significant, causing a large horizontal spread of the plume, especially close to the surface (Figure 8).

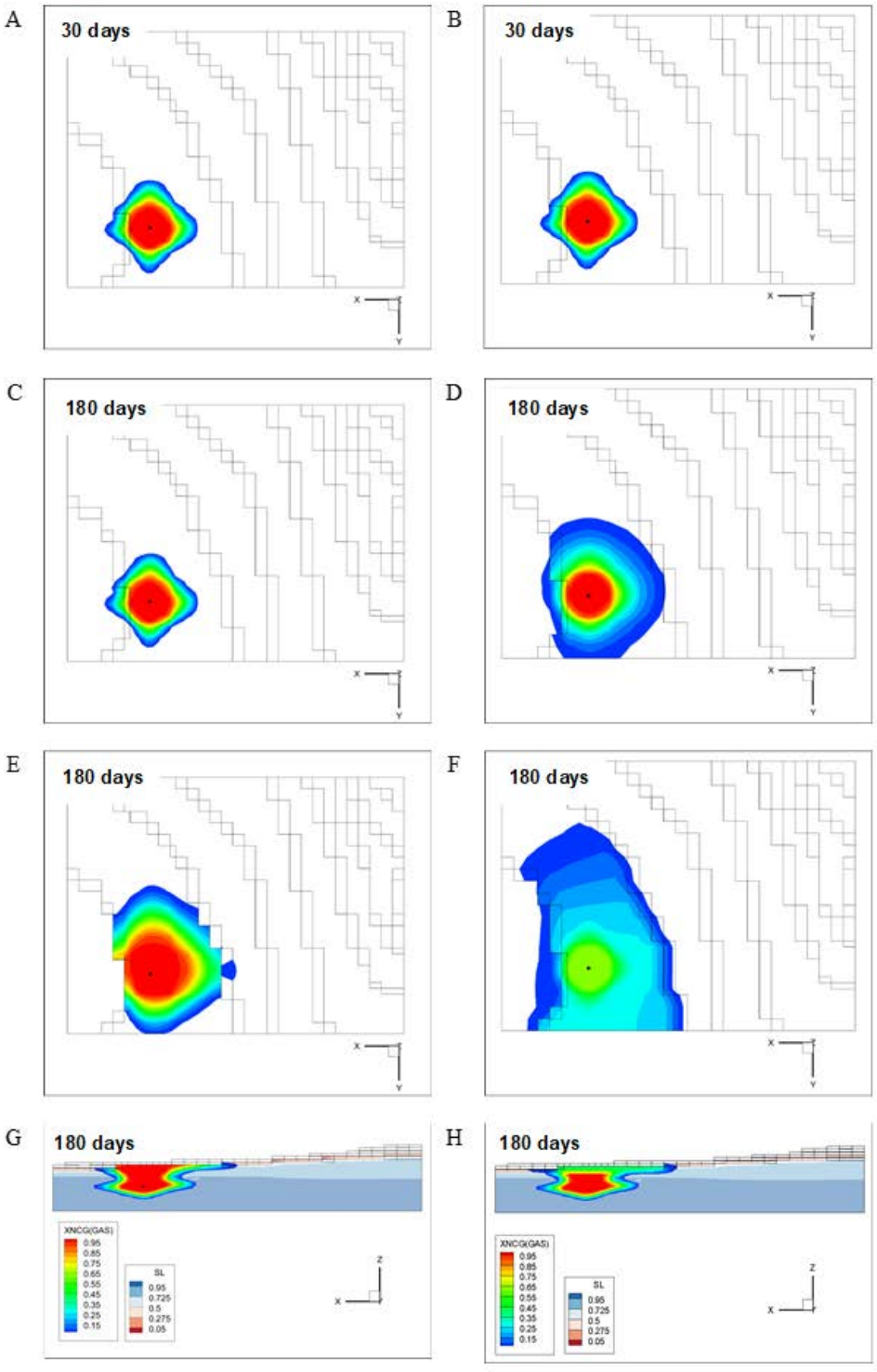

Figure 8. CO_2 mass fraction in the gas phase at 30 days (A and B) and 180 days (C–H) for simulations without diffusion (left column) and with diffusion included (right column). (A–D) Horizontal cross-sections at injection point; (C and E) horizontal cross-section at surface; (G and H) vertical cross-section at injection point (SL, liquid phase saturation)

Sediment permeability anisotropy was tested by both increasing the horizontal permeabilities (k_x and k_y) 10-fold, and also reducing the vertical permeability (k_z) by the same order of magnitude. These resulted in significant changes in the plume shape as expected. The first case (horizontal increase) yielded a much more horizontal spread, causing the CO_2 to barely reach the surface in 30 days (Figure 9B). On the other hand, the plume was more round-shaped when *z*-permeability is reduced 10-fold – even the transition "throat" between layers is less pronounced in this case (Figure 9C).

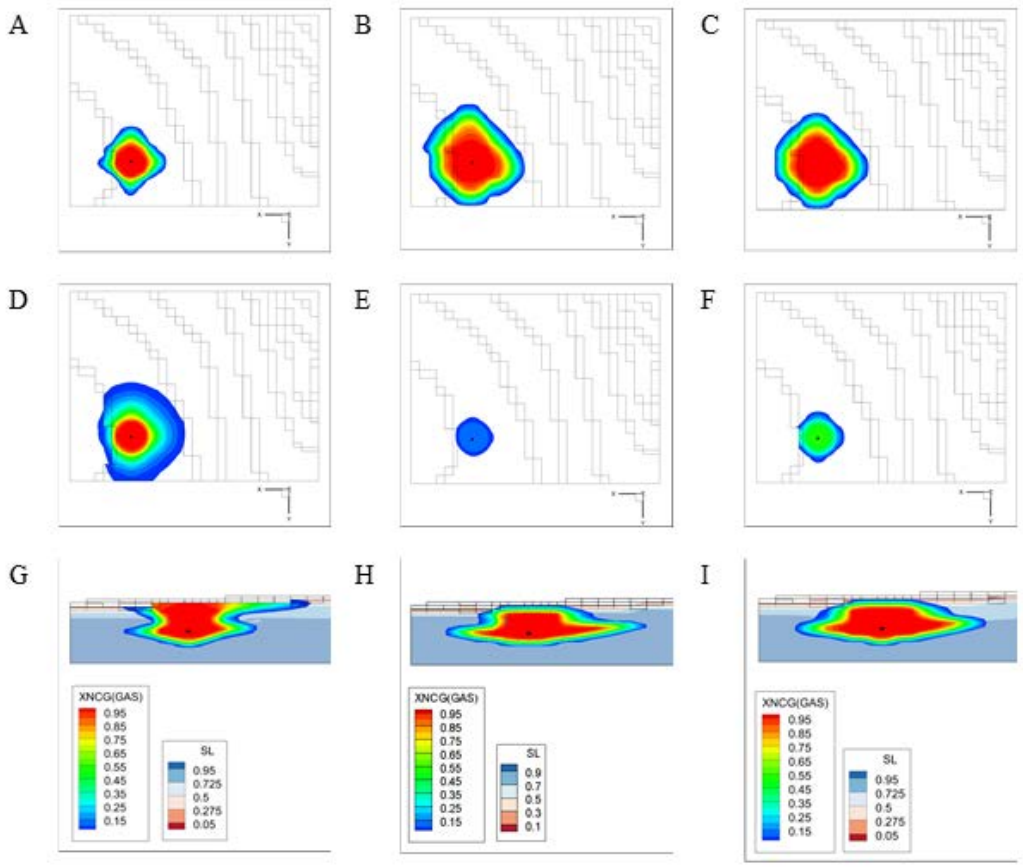

Figure 9. CO_2 mass fraction in the gas phase at 30 days for simulation with isotropic permeability (left column); 10-fold increase in the horizontal direction (center column) and 10-fold decrease in the vertical direction (right column). (A–C) Horizontal cross-section at injection point; (D–F) horizontal cross-section at the surface; (G–I) vertical cross-section at injection point (SL, liquid phase saturation)

Comparing the results of the simulations carried out with the open *versus* closed top boundary, it was observed that the overall shape of the CO_2 plume is not significantly

affected – in both cases, it shows the clear division between the silt and clay layers, although the with the open boundary model the plume is more spread in all directions, specially closer to surface (Figure 10). This is expected considering that with the closed system the injected gas will create a higher overpressure (specially in this case where injection occurs in a saturated zone), restricting its movement. In both cases the plume is nearly unchanged after injection stops (no diffusion considered) (Figure 10C/10D).

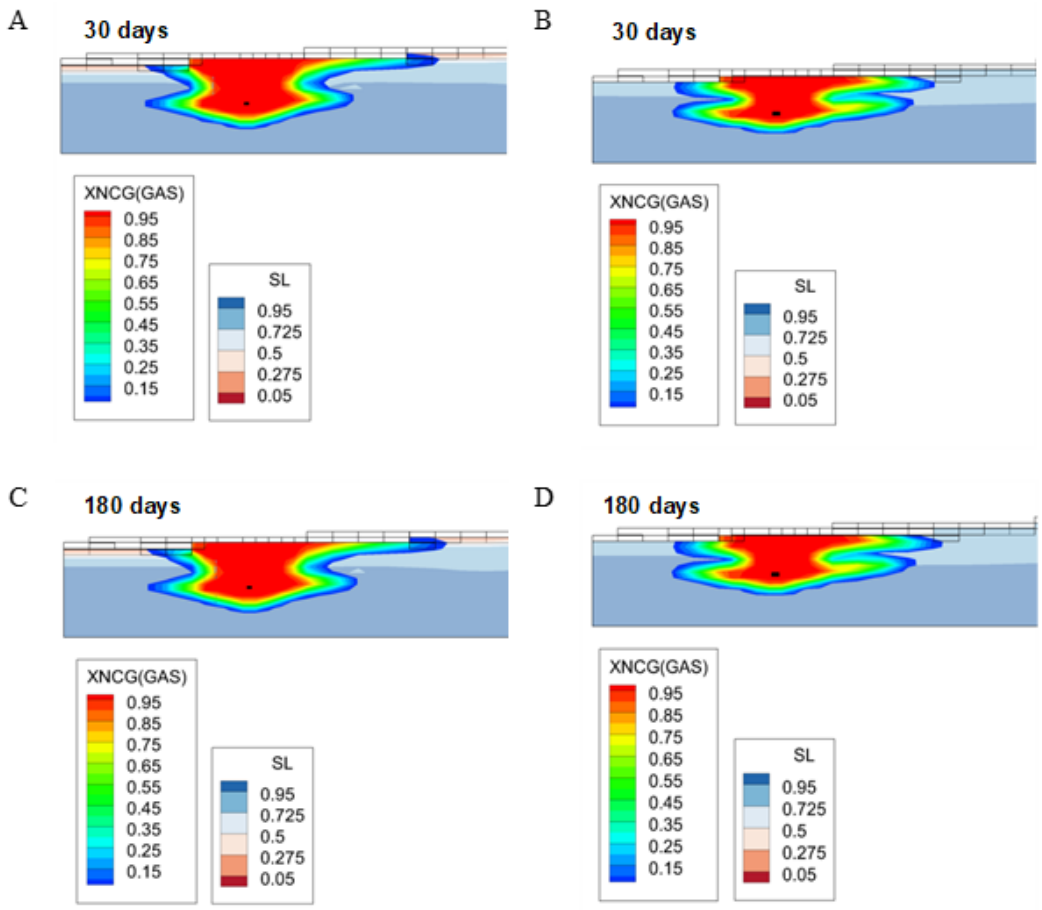

Figure 10. CO_2 mass fraction in the gas phase at 30 and 180 days for simulation with open (left column) and closed (right column) top boundary.

Mass balances of CO_2 in the system, in both aqueous and gas phase, over time are plotted in Figure 11. For the closed model, CO_2 amount increases linearly up to 600 kg, as expected (30 days of injection at a rate of 20 kg/day). In the open-boundary model with isotropic permeabilities, the amount of CO_2 starts deviating from linearity in ca. 7-8 days after

injection onset, indicating that the plume has reached the top and CO_2 starts flowing out to the atmosphere, continuing after injection stops. The amount of CO_2 in the system peaks at 30 days, with ca. 370 kg, and stabilizes at approximately 310 kg – slightly over 50% of the total amount injected. With anisotropic permeabilities, the amount of CO_2 remaining in the system is much higher, as the flow is restricted by the permeability conditions imposed. After the injection period, approximately 97% of the injected gas still remains underground. After injection stops, CO_2 keeps slowly flowing out to the atmosphere, stabilizing at ca. 542 kg (around 90% of the injected amount).

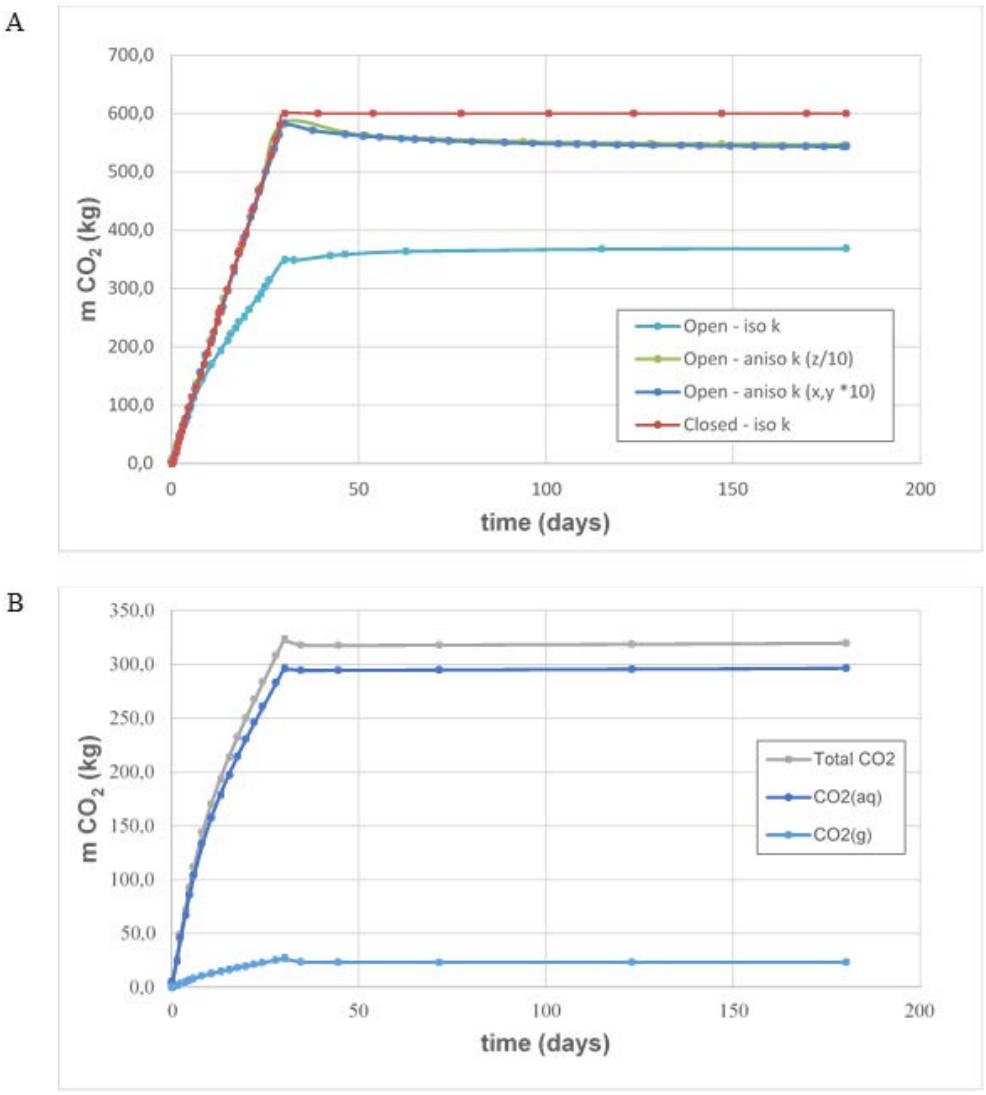

Figure 11. Total mass of CO_2 in the system with time for the simulations (including diffusion) with closed and open top boundaries (with different permeabilities) (A) and CO_2 phase distribution over time for the open top boundary model, isotropic permeability (no diffusion) (B)

In all simulations, most of the injected CO_2 dissolves into the aqueous phase soon after injection (Figure 11B). This is not unexpected, analyzing the model dimensions and conditions. Considering that a grid block contains approximately 1000 kg of water (2.7 m^3 times an average porosity of 0.35), and the CO_2 solubility is ca. 1.7 g/kg of water, a single cell can dissolve approximately 1700 kg of CO_2, almost three times the total amount injected. Dissolution occurs very fast, as can be observed in Figure 11B – after injection stops,

maximum dissolution is reached in less than 5 days, and the system reaches phase distribution equilibria. Of all CO_2 remaining in the system, approximately 95% is dissolved in water, with only 5% in the gas phase.

Table 3 summarizes some key findings from the simulations. The results show the high sensitivity to permeability, with anisotropic condition resulting in a much higher retention and longer times to reach the surface (approximately 16-19 days). Diffusions influences slightly on the plume dispersion after injection stops (an additional 1 m spread from 30 to 180 days). With a closed system, the plume is less dispersed in the beginning due to higher overpressure. In the end (180 d) it is more distributed along top layers (ca. 2 m more than the open system), as fluids are unable to flow out of the model. CO_2 dissolves rapidly, and the mass fraction in solution does not change significantly after injection stops. Models with anisotropic permeability present a slightly higher percentage of CO_2 in solution, due to a higher lateral spread and longer time of retention underground, compared to isotropic models. These models also present the higher retention of CO_2, and loss after injection stops (ca. 9.3% released after 30 days). Interestingly, the isotropic model with diffusion, which has a high initial loss (58%), has a flow back of CO_2 from the atmosphere into the sediment (ending with ca. 61% of the total injected amount).

Table 3: Summary of results for each model considered in this study.

Model			Time to reach surface (days)	CO_2(g) dispersion in *x*-direction after 30 days (meters)[a]	CO_2(g) dispersion in *x*-direction after 180 days (meters)[a]	% CO_2(aq) after 30 d	% CO_2(aq) after 180 d	Total CO_2 (kg) after 30 days	Total CO_2 (kg) after 180 days
Top boundary	**Diffusion**	**Permeability**							
open	no	isotropic ($k_x = k_y = k_z$)	3.6	26.5 (silt layer)	26.5 (silt layer)	91.7	92.7	323.05	319.60
open	yes	isotropic ($k_x = k_y = k_z$)	2.5	26.5 (silt layer)	27.5 (silt layer)	91.2	91.9	349.08	368.73
open	yes	anisotropic (k_x, k_y x 10)	16.5	28.5 (clay layer)	29.0 (clay layer)	93.8	96.0	582.22	543.23
open	yes	anisotropic (k_z/10)	18.5[b]	26 (clay layer)	26 (clay layer)	92.8	95.1	583.87	546.24
closed	yes	isotropic ($k_x = k_y = k_z$)	2.3	24 (silt layer)	29.5 (silt layer)	91.0	91.5	600.00	600.00

[a]measured at minimum of 5% of CO_2 mass fraction in gas phase

Field results from the CO_2 flow monitoring into the atmosphere carried out after injection stop revealed almost no gas release from the soil, with very small amounts being detected around the injection well (Figure 12)[35]. From the simulation results, the condition that models that approximates better with this observation are those considering anisotropic permeabilities, either by an increase in the *x*- and *y*-direction or decrease in the *z*-direction, as seen in Figure 9E/9F.

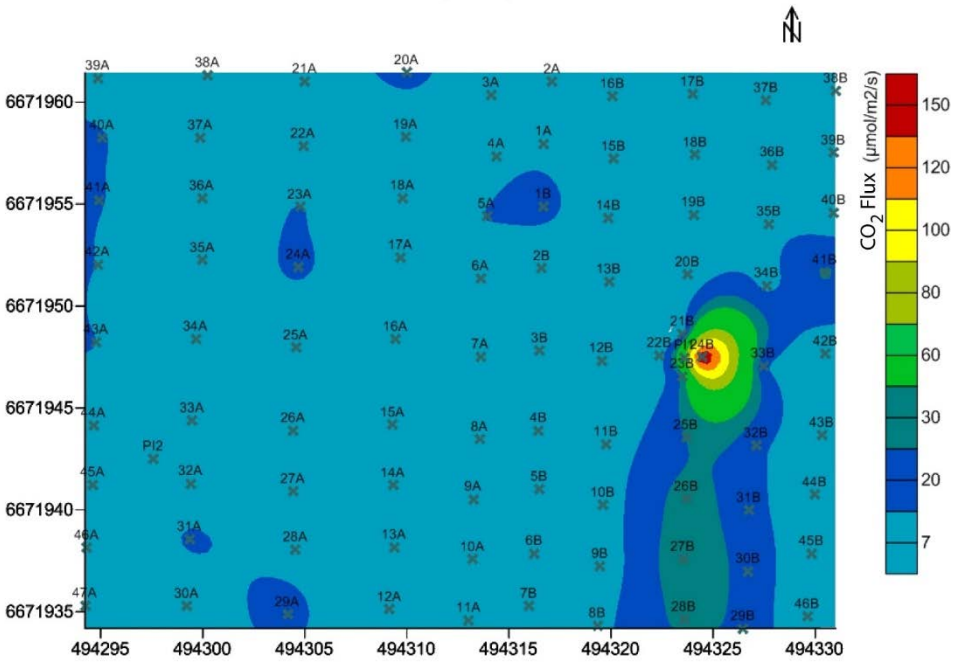

Figure 12. CO_2 molar flow rate in the soil–atmosphere interface measured in the field at the last day of injection (cross-marks indicate flow chamber positions, axis indicate UTM coordinates) (adapted from Melo et al.[35]).>

Preliminary results from resistivity changes measured in the fields after 30 days from injection start are shown in Figure 13. These changes can be associated with the alterations due to CO_2 injection, and the results suggest a much wider spread of the CO_2 within the field, compared to the model results, where it is confined to the vicinity of the well. As in the simulation results, the horizontal flow appears to be dominant as well. The vertical plot shows very small alterations near the surface. The higher changes are close to the injection well, and ca. 20-25 m to the west - in agreement with the measured flow in the soil-atmosphere interface and the model results (Figure 13).

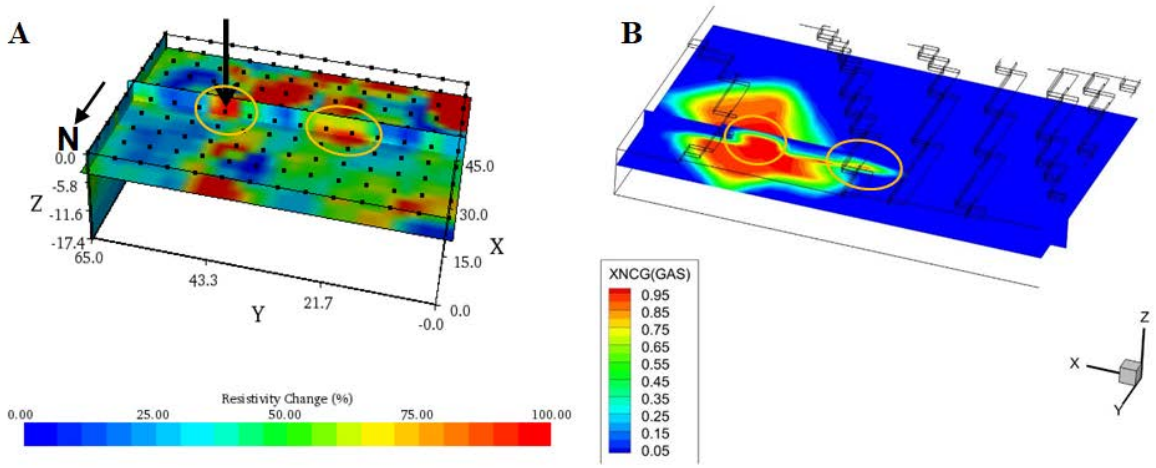

Figure 13. (A) Resistivity change (%) measured in the field and (B) calculated CO_2 mass fraction in the gas phase, after 30 days of CO_2 injection start. Simulations with open top boundary including diffusion and anisotropic permeability (kx, ky × 10). Circles highlight regions of high CO_2 saturation close to the surface.>

The measured resistivity changes indicates strong heterogeneities are present in the field, with regions with low porosity/high permeabilities that enhance CO_2 flow further away from the injection well. These features were not present in the current model, based in the existing data from the field, which explains in part the observed differences. New field data collection is under way, with more sampling points and analytical techniques, that will refine the geological model for future simulations. With improved refined models that include medium heterogeneities, other simulation conditions such as the consideration of lateral flows, rainfall events and/or temperature variations, and the inclusion of perched water bodies will also be tested. With better matching between field data and model results, longer simulation times can also be considered, in order to predict the long-term (years or decades) fate of the leakage scenario.

4. Conclusions

This paper presents the results of a numerical modeling study carried out under the CO_2MOVE controlled release experimental project. The study evaluated the influence of various model parameters and conditions that are likely to affect the system response, such as diffusion, permeability, and boundary conditions. The inclusion of diffusion in the model proved to be important to ensure some CO_2 mobility after injection stops, in the absence of other continuing perturbations. Permeability anisotropy was revealed to play an important role – results indicated that a 10-fold increase in the horizontal permeabilities give a better approximation to the field results, which showed quite small leakage of CO_2 to the atmosphere, confined to the vicinity of the injection well.

Mass balances were used to estimate the amount of CO_2 leaving the system over time. It was found that this amount is quite sensitive to permeability parameters used in the model. When anisotropic permeability conditions were applied, the flow of CO_2 out of the system is significantly reduced, which is in better agreement with the observed field results. Most of the injected CO_2 is rapidly dissolved in the pore water, with approximately 5% remaing in gas phase. The fractions of CO_2 remaining in the subsurface and escaping to the atmosphere vary significantly with the tested parameters. With anisotropic permeability, most of it stays trapped in the soil (more than 90%).

Overall, the results were consistent with the expected CO_2 behavior in the study area considering a geological framework homogeneously distributed with a free aquifer. With higher permeabilities in the horizontal direction, the injected CO_2 was shown to seep slowly and reach the surface in approximately two weeks, around the injection well, as observed with in the field with installed soil flux chambers. Nevertheless, additional field data and model refinements could provide an even better reproduction of the system, further improving future models.

5. Acknowledgements

This study had financial support from PETROBRAS and CAPES, and has been developed in the Institute of Petroleum and Natural Resources – IPR, at the Pontifical Catholic University of Rio Grande do Sul – PUCRS, Porto Alegre, Brazil.

6. References

1. Ketzer JM, Iglesias RS, Einloft S. Reducing Greenhouse Gas Emissions with CO2 Capture and Geological Storage. In: Chen W-Y, Suzuki T, Lackner M, editors. Handbook of Climate Change Mitigation and Adaptation [Internet]. 2nd ed. New York, NY: Springer New York; 2015. p. 1–40. Available from: http://dx.doi.org/10.1007/978-1-4614-6431-0_37-2
2. IPCC. Special Report on Carbon Dioxide Capture and Storage. Metz B, Davidson O, de Coninck H, Loos M, Meyer L, editors. New York, USA: Intergovernmental Panel on Climate Change; 2005.
3. Holloway S. An overview of the underground disposal of carbon dioxide. Energy Convers Manag [Internet]. 1997;38:S193–8. Available from: http://www.sciencedirect.com/science/article/B6V2P-4DS9V40-15/2/2a34679500a7a82f2af77314263dfb4f
4. Benson SM, Bennaceur K, Cook P, Davison J, de Coninck H, Farhat K, et al. Chapter 13 - Carbon Capture and Storage. In: Global Energy Assessment - Toward a Sustainable Future [Internet]. Cambridge University Press, Cambridge, UK and New York, NY, USA and the International Institute for Applied Systems Analysis, Laxenburg, Austria; 2012. p. 993–1068. Available from: www.globalenergyassessment.org
5. Bui M, Adjiman CS, Bardow A, Anthony EJ, Boston A, Brown S, et al. Carbon capture and storage (CCS): The way forward. Energy Environ Sci [Internet]. 2018;11(5):1062–176. Available from: http://dx.doi.org/10.1039/C7EE02342A
6. Bradshaw J, Bachu S, Bonijoly D, Burruss R, Holloway S, Christensen NP, et al. CO2 storage capacity estimation: Issues and development of standards. Int J Greenh Gas Control. 2007;1:62–8.
7. Roberts JJ, Stalker L. What have We Learned about CO2 Leakage from Field Injection Tests? Energy Procedia [Internet]. 2017;114(November 2016):5711–31. Available from: http://dx.doi.org/10.1016/j.egypro.2017.03.1710
8. Arts R, Winthaegen P. Monitoring Options for CO2 Storage. In: Benson SM, editor. Carbon Dioxide Capture for Storage in Deep Geologic Formations – Results from the CO2 Capture Project Vol 2. Amsterdam: Elsevier; 2005. p. 1001–14.
9. Cawley S V, Saunders MR, Le Gallo Y, Carpentier B, Holloway S, Kirby GA, et al. The NGCAS Project—Assessing the Potential for EOR and CO2 Storage at the Forties Oilfield, Offshore UK. In: Benson SM, editor. Carbon Dioxide Capture for Storage in Deep Geologic Formations – Results from the CO2 Capture Project Vol 2. Amsterdam: Elsevier; 2005. p. 713–50.
10. Jenkins C, Chadwick A, Hovorka SD. The state of the art in monitoring and verification—Ten years on. Int J Greenh Gas Control [Internet]. 2015 Jun [cited 2015 Aug 26];40:312–49. Available from: http://www.sciencedirect.com/science/article/pii/S1750583615001723
11. Arts R, Eiken O, Chadwick A, Zweigel P, van der Meer L, Zinszner B. Monitoring of CO2 injected at Sleipner using time-lapse seismic data. Energy [Internet]. 2004;29:1383–92. Available from: http://www.sciencedirect.com/science/article/B6V2S-4CC7RP3-V/2/20402b4eb8351a930551b5ef0f535e99
12. Zhu C, Zhang G, Lu P, Meng L, Ji X. Benchmark modeling of the Sleipner CO2 plume: Calibration to seismic data for the uppermost layer and model sensitivity analysis. Int J Greenh Gas Control [Internet]. 2015;43:233–46. Available from:

http://www.sciencedirect.com/science/article/pii/S1750583614003958
13. Hansen O, Gilding D, Nazarian B, Osdal B, Ringrose P, Kristoffersen J-B, et al. Snøhvit: The History of Injecting and Storing 1 Mt CO2 in the Fluvial Tubåen Fm. Energy Procedia [Internet]. 2013;37:3565–73. Available from: http://www.sciencedirect.com/science/article/pii/S187661021300492X
14. Chadwick A, Arts R, Eiken O, Williamson P, Williams G. GEOPHYSICAL MONITORING OF THE CO2 PLUME AT SLEIPNER, NORTH SEA. In: Lombardi S, Altunina LK, Beaubien SE, editors. Advances in the Geological Storage of Carbon Dioxide [Internet]. Dordrecht, Netherlands: Springer; 2006. p. 303–14. (NATO Science Series; vol. IV. Earth). Available from: http://dx.doi.org/10.1007/1-4020-4471-2_25
15. Dixon T, Romanak KD. Improving monitoring protocols for CO2 geological storage with technical advances in CO2 attribution monitoring. Int J Greenh Gas Control [Internet]. 2015;41:29–40. Available from: http://www.sciencedirect.com/science/article/pii/S1750583615001929
16. Spangler LH, Dobeck LM, Repasky KS, Nehrir AR, Humphries SD, Barr JL, et al. A shallow subsurface controlled release facility in Bozeman, Montana, USA, for testing near surface CO2 detection techniques and transport models. Environ Earth Sci [Internet]. 2010;60(2):227–39. Available from: https://doi.org/10.1007/s12665-009-0400-2
17. Feitz A, Jenkins C, Schacht U, McGrath A, Berko H, Schroder I, et al. An assessment of near surface CO2 leakage detection techniques under Australian conditions. Energy Procedia [Internet]. 2014;63:3891–906. Available from: http://www.sciencedirect.com/science/article/pii/S1876610214022346
18. Jones DG, Barkwith a. K a P, Hannis S, Lister TR, Gal F, Graziani S, et al. Monitoring of near surface gas seepage from a shallow injection experiment at the CO2 Field Lab, Norway. Int J Greenh Gas Control [Internet]. 2014;28:300–17. Available from: http://dx.doi.org/10.1016/j.ijggc.2014.06.021
19. Cohen G, Loisy C, Laveuf C, Le Roux O, Delaplace P, Magnier C, et al. The CO2-Vadose project: Experimental study and modelling of CO2 induced leakage and tracers associated in the carbonate vadose zone. Int J Greenh Gas Control [Internet]. 2013;14:128–40. Available from: http://www.sciencedirect.com/science/article/pii/S1750583613000145
20. van der Zwaan B, Gerlagh R. Economics of geological CO2 storage and leakage. Clim Change [Internet]. 2009;93(3):285–309. Available from: https://doi.org/10.1007/s10584-009-9558-6
21. Hepple RP, Benson SM. Geologic storage of carbon dioxide as a climate change mitigation strategy: performance requirements and the implications of surface seepage. Environ Geol [Internet]. 2005;47(4):576–85. Available from: https://doi.org/10.1007/s00254-004-1181-2
22. Lofi J, Pezard P, Bouchette F, Raynal O, Sabatier P, Denchik N, et al. Integrated Onshore-Offshore Investigation of a Mediterranean Layered Coastal Aquifer. Groundwater [Internet]. 2013 Jul 1;51(4):550–61. Available from: https://doi.org/10.1111/j.1745-6584.2012.01011.x
23. Gasparini A, Credoz A, Grandia F, Garcia DA, Bruno J. Experimental and numerical modeling of CO2 leakage in the vadose zone. Greenh Gases Sci Technol. 2015;5(6):732–55.
24. Ko D, Yoo G, Yun S-T, Chung H. Impacts of CO2 leakage on plants and microorganisms: A review of results from CO2 release experiments and storage sites. Greenh Gases Sci Technol [Internet]. 2016 Jun 1;6(3):319–38. Available from: https://doi.org/10.1002/ghg.1593
25. Oldenburg C, Lewicki J, Dobeck L, Spangler L. Modeling Gas Transport in the Shallow Subsurface During the ZERT CO2 Release Test. Transp Porous Media [Internet]. 2009; Available from: http://dx.doi.org/10.1007/s11242-009-9361-x
26. Basirat F, Niemi A, Perroud H, Lofi J, Denchik N, Lods G, et al. Modeling gas transport in the shallow subsurface in maguelone field experiment. Energy Procedia [Internet]. 2013;40:337–45. Available from: http://dx.doi.org/10.1016/j.egypro.2013.08.039
27. Parkhurst DL, Appelo CAJ. User's guide to PHREEQC (version 2)—A computer program for speciation, batch-reaction, one-dimensional transport, and inverse geochemical calculations. U.S. Geological Survey Water Resources Investigations; 1999.
28. Humez P, Négrel P, Lagneau V, Lions J, Kloppmann W, Gal F, et al. CO2-water-mineral reactions during CO2 leakage: Geochemical and isotopic monitoring of a CO2 injection field test. Chem Geol [Internet]. (0). Available from: http://www.sciencedirect.com/science/article/pii/S0009254114000242
29. Melo CL, De Moreira AC, Goudinho FS, Bressan LW, Constant MJ, Oliva A, et al. CO2MOVE Project: The New Brazilian Field Lab Fully Dedicated to CO2MMV Experiments. Energy Procedia [Internet]. 2017;114(November 2016):3699–715. Available from:

http://dx.doi.org/10.1016/j.egypro.2017.03.1501
30. Oldenburg CM. EOS7CA Version 1.0: TOUGH2 Module for Gas Migration in Shallow Subsurface Porous Media Systems. 2015.
31. Unger AJA, Oldenburg CM. On Leakage and Seepage from Geologic Carbon Sequestration Sites: Unsaturated Zone Attenuation. Vadose Zo J [Internet]. 2003 Aug 1;2(3):287–96. Available from: https://doi.org/10.2113/2.3.287
32. Pruess K, Oldenburg C, Moridis G. TOUGH2 User's Guide, Version 2.1 [Internet]. Berkeley, CA: Lawrence Berkeley National Laboratory; 2011. Available from: http://esd.lbl.gov/TOUGH2
33. Alan Freeze R, A Cherry J. Groundwater. 1st ed. Prentice-Hall; 1979. 604 p.
34. Saxton KE, Rawls WJ. Soil water characteristic estimates by texture and organic matter for hydrologic solutions. Soil Sci Soc Am J. 2006;70(5):1569–78.
35. Melo CL, Goudinho FS, Bressan LW, Constant MJ, Augustin AH, Iglesias RS, et al. CO2MOVE Project: testing CO2 monitoring methods for onshore CCS. In: 14th Greenhouse Gas Control Technologies Conference (GHGT-14). Melbourne: SSRN; 2018.